Mechanism and Control of Anthropomorphic Biped Robots

Hun-ok Lim[1,2] & Atsuo Takanishi[2,3]
[1]Department of Mechanical Engineering, Kanagawa University
[2]Humanoid Robotics Institute, Waseda University
[3]Department of Mechanical Engineering, Waseda University

1. Introduction

Human beings, animals and some birds use their legs to move with great mobility, but we do not yet have a full understanding of their motion mechanism. The reason is that we lack man-made robots that use legs to obtain high mobility. We, especially, need two-legged robots that are able to adapt to human living environments such as offices and homes.

In order to analyze a human walking mechanism, some research groups studied about hydraulically-actuated or pneumatically-activated two-legged mechanisms in the 1960s. In 1973, a world's first full-scale anthropomorphic robot, WABOT-1 (WAseda roBOT-1), was constructed at Waseda University as shown in Figure 1. It was able to communicate with a human in Japanese and to measure the distance and direction of objects using external receptors such as an artificial mouth, ears and eyes (Kato *et al.*, 1973). Hydraulically powered, it used disproportionately large feet for stability. Also, it was able to grip and carry objects using the hands that were equipped with tactile sensors.

In 1983, WL-10R (Wasada Leg-10 Refined) was constructed using rotary type servo-actuators and carbon-fiber reinforced plastic. It was able to walk forwards and backwards, and turn on a flat plane. Based on the WL-10R, WHL-11 was developed by Wasada and Hitachi (Takanishi *et al.*, 1985). It walked more than 85 km at Tsukuba Science Expo'85. In 1986-1995, WL-12 series robots that have a trunk and a 2-DOF waist was constructed to simulate human walking motion including his upper body motion as shown in Figure 2 (Takanishi *et al.*, 1988; Li *et al.*, 1992; Yamaguchi *et al.*, 1995). They performed dynamic walking going up and down a stair with a height of 0.1 m and a slope of 10 deg (Takanishi *et al.*, 1990). Also, they did not fall down and walked under an unknown external force of 100 N applied to their backs (Takanishi *et al.*, 1991). However, the relative motion between their upper body and legs was difficult to be simulated.

An electrically powered human-sized biped humanoid robot, WABIAN (WAseda BIped humANoid), was constructed in 1996 for simulating human motion. It consists of a total of 35 DOF; two 3-DOF legs, two 10-DOF arms, two 2-DOF eyes, a 2-DOF neck and a torso with a 3-DOF waist (Setiawan *et al.*, 1999). After 1996, WABIAN series robots were developed, and achieved qusi-human follow walking, emotional motion, dancing motion and so on (Setiawan *et al.*, 1999; Lim *et al.*, 2004a).
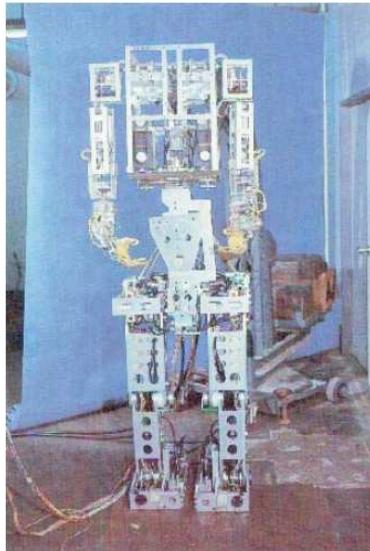
Fig. 1. Photo of WABOT-1.

Section 2 deals with the mechanism and software of WABIAN-RII (WAseda BIped humANoid-Refined II). The WABIAN-RII is a full-scaled biped humanoid robot that has 43 mechanical degrees of freedom (DOF). Section 3 addresses a locomotion pattern generation for biped humanoid robots. Its locomotion pattern is created online or offline according to the terrain conditions. Section 4 describes moment compensation control that is based on the motion of the waist and trunk. The motion of the waist and trunk is applied to maintain a good balance of the whole robot's body while the path of the legs is controlled according to the terrain. Section 5 describes impedance control to reduce the contact/impact force of the landing foot. Impedance parameters are changed in real time depending on the gait phase. Section 6 addresses walking experiments to verify the effectiveness of the mechanism of the WABIAN serious robots, the moment compensation control and the impedance control. Section 7 describes conclusions. Also, future works are discussed to make more reliable control systems.

2. Mechanisms of WABIAN-RII

An adult-sized humanoid robot should be constructed to properly simulate human motion. We have been developing WABIAN-series robots since 1996. In this section, the mechanical and electrical structure of WABIAN-RII is proposed.

2.1 Mechanical Mechanisms

WABIAN-RII consists of two 6-DOF legs, two 7-DOF arms, two 3-DOF hands, two 2-DOF eyes, a 4-DOF neck and a torso with a 3-DOF waist (Lim *et al*., 2004a). Table 1 shows DOF of WABIAN-RII. Figure 3 shows a photo of WABIAN-RII. Its height is 1840 mm and its total weight is 127 kg. Table 2 and Table 3 show the weight and length distribution of each segment, respectively. The movable angle of the waist's roll and yaw is ± 20 deg and ± 45

deg, respectively. The movable angle of the waist's pitch is + 30 deg and -10 deg. The movable angle of the knee is + 90 deg and - 0 deg. Figure 4 shows the movable angles of the pitch, roll and yaw, respectively. Duralumin, GIGAS (YKK Corp.) and CFRP (Carbon Fiber Reinforced Plastic) are mainly employed as its structural materials.
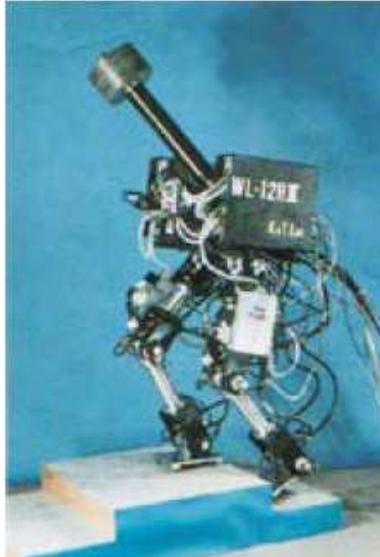

Fig. 2. Photo of WL-12RIII.

Fig. 3. Photo of WABIAN-RII.

2.2 Electrical systems

The trunk and legs of WABIAN-RII are driven by AC servo motors with reduction gears. The neck, hands and arms are actuated by DC servo motors with reduction gears. The eyes are driven by DC servo motors without reduction gears. Two CCD cameras that are attached to the head observe human environments. A force/torque sensor is attached to the wrist to detect interaction, and another force/torque sensor is attached between the ankle and the foot to measure ZMP. Also, a voice recognition system is installed.

WABIAN-RII is controlled by a PC/AT compatible computer PEAK-530 (Intel MMX Pentium 200 MHz CPU processor) run by MS-DOS 6.2/V (16-bit). TNT DOS-Extender SDK (Ver.6.1) is employed to extend the OS to a 32-bit. It has three counter boards, each with 24-bit 24 channels, three D/A converter boards, each with 12-bit 16 channels and an A/D converter board with differential 12-bit 16 channels to interface with sensors. The joint angles are sensed by incremental encoders attached to the joints, and the data are transferred to the computer through the counters. All the computations to control WABIAN-RII are carried out by the central computer, which runs the control program written in C language. The servo rate is 1 kHz. The computer system is mounted on the back of the waist and the servo driver modules are mounted on the upper part of the trunk. Electric power is the only external connection. Figure 5 shows the control system of WABIAN-RII.

Parts	DOF
Eye	2 (1 pitch, 1 yaw) × 2
Neck	4 (2 pitch, 1 roll, 1 yaw)
Waist	3 (1 pitch, 1 roll, 1 yaw) × 2
Hip	3 (1 pitch, 1 roll, 1 yaw) × 2
Knee	1 (1 pitch) × 2
Ankle	2 (1 pitch, 1 roll) ×2
Shoulder	3 (1 pitch, 1 roll, 1 yaw) × 2
Albow	1 (1 pitch)
Wrist	3 (1 pitch, 1 roll, 1 yaw) × 2
Hand	3 (thumb 1-DOF, index finger 1-DOF, the other fingers 1-DOF) × 2

Table 1. DOF of WABIAN-RII.

Parts	Weight (kg)	Parts	Weight (kg)
Foot	1.9 (×2)	Hand	0.5 (×2)
Ankle	7.8 (×2)	Wrist	0.5 (×2)
Knee	5.3 (×2)	Elbow	0.9 (×2)
Head	2.4	Shoulder	5.9 (×2)
Neck	6.4	Waist	20.6
Trunk	52.0		

Table 2. Segment weight of WABIAN-RII.

Parts	Length (mm)
Height	1840
Width	706
Depth	533
Between foot and ankle	142
Between ankle and knee	300
Between knee and hip	353
Between hip and waist	176
Between waist and neck	537
Between neck and head	332
Upper arm	263
Lower arm	247

Table 3. Segment length of WABIAN-RII.

(a) Pitch's movable angle   (b) Roll's movable angle

(c) Yaw's movable angle
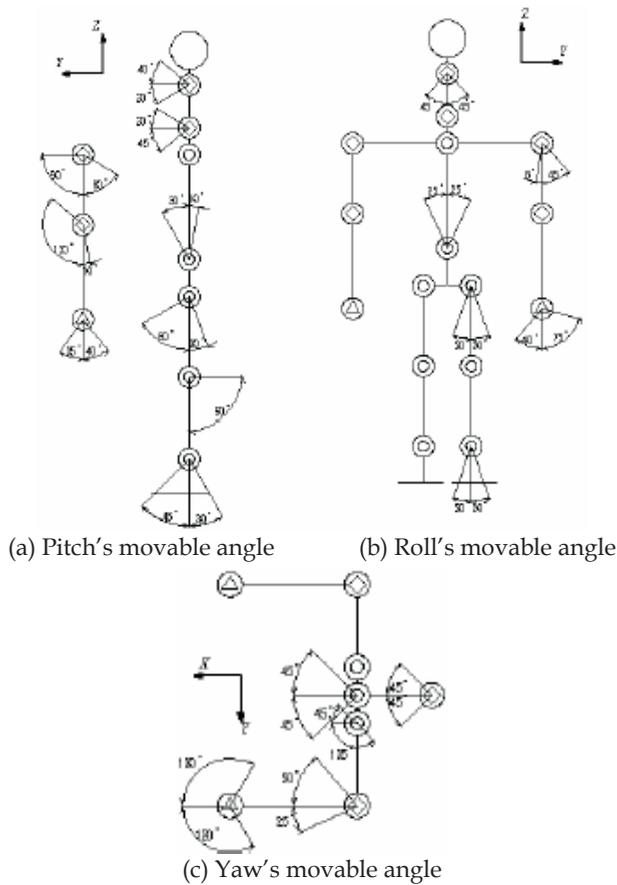
Fig. 4. Movable range of WABIAN-RII.
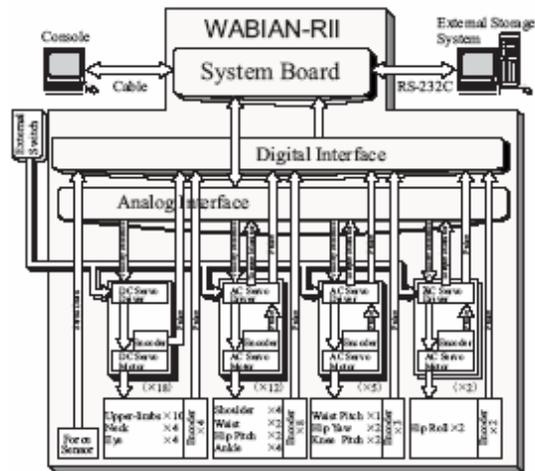
Fig. 5. Control system of WABIAN-RII.

3. Locomotion Pattern Generation

A biped locomotion phase can be classified into a contact, a single and a double supporting phase to generate a leg motion. During the single supporting phase, one foot is not constrained to the ground but the other foot is on the ground. As soon as the heel of the swinging foot reaches the ground, the single supporting phase is changed to the contact phase. If the toe and heel of the swinging foot contacts on the ground, the phase becomes a double supporting phase. Fig. 6 shows a locomotion phase for a leg pattern generation.

The smooth motion of the foot according to terrain conditions, x_f, can be generated by using a sixth degree polynomial considering the angle, the angular velocity, the angular acceleration and the height from the ground to the foot (Lim *et al.*, 2004b). Three constraints of the foot position and orientation come from the selection of initial and final values:

$$x_f(t_0) = x_0, \ x_f(t_f) = x_f, \ x_f(t_m) = x_m, \tag{1}$$

where t_0, t_m and t_f are the initial, intermediate and final time of a step, respectively.

The position and orientation of the foot have an additional four constraints that are the zero initial and final velocity and acceleration:

$$\dot{x}_f(t_0) = 0, \ \dot{x}_f(t_f) = 0, \ \ddot{x}_f(t_0) = 0, \ \ddot{x}_f(t_f) = 0. \tag{2}$$

The sixth order polynomial for a foot motion is written as follows:

$$x_f(t) = a_0 + a_1 t + a_2 t^2 + a_3 t^3 + a_4 t^4 + a_5 t^5 + a_6 t^6, \tag{3}$$

and the velocity and acceleration along the path are clearly

$$\begin{aligned} \dot{x}_f(t) &= a_1 + 2a_2 t + 3a_3 t^2 + 4a_4 t^3 + 5a_5 t^4 + 6a_6 t^5, \\ \ddot{x}_f(t) &= 2a_2 + 6a_3 t + 12a_4 t^2 + 20a_5 t^3 + 30a_6 t^4. \end{aligned} \tag{4}$$

Combining Equation (3) and Equation (4) with the seven constraints, the seven coefficients ($a_0 \cdots a_6$) can be obtained. Then, substituting these coefficients for Equation (3), the foot motion pattern is obtained. In addition, a knee and waist pattern is created by inverse kinematics.
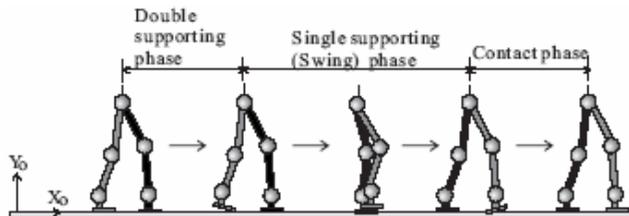

Fig. 6. Locomotion phase.

4. Moment Compensation Control

When a biped humanoid robot walks, moments generated by the motion of the legs make it unstable (Lim & Takanishi, 2005). To cancel the moments, a moment compensation control is discussed in this section.

4.1 Concept of Zero Moment Point
Consider a single supporting phase in which one foot is not constrained to the ground. As shown in Figure 7, the supporting polygon (stable region) is made by the contact points between the foot sole and the ground. To maintain the dynamic equilibrium of a biped humanoid robot, the ground reaction force should act at an appropriate point on the foot sole. It means that the ZMP (Zero Moment Point) exists at a point where the total forces and moments are equal to zero in the support polygon (Vukobratovic *et al.*, 1970). In this study, the ZMP is arbitrarily set in the stable region.
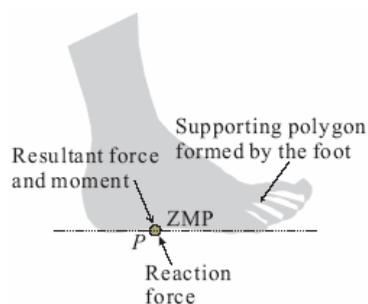

Fig. 7. ZMP in supporting polygon.

4.2 Moment Compensation
A world coordinate frame $\mathcal{F}$ is fixed on the ground, and a moving coordinate frame $\bar{\mathcal{F}}$ is attached to the center of the waist of a biped humanoid robot to define mathematical quantities. Considering that the humanoid robot is a set of particle model, the balancing moment around a contact point p in a supporting polygon can be expressed with respect to the world coordinate frame $\mathcal{F}$ as

$$\sum_{i=1}^{n} m_i(r_i - r_p) \times (\ddot{r}_i + G) + T - \sum_{j=1}^{n}((r_j - r_p) \times F_j + M_j) = 0, \tag{5}$$

where r_p is the position vector of the point p from the origin of the frame $\mathcal{F}$. m_i is the mass of the particle i of the biped humanoid robot. r_i and $\ddot{r}_i$ denote the position and acceleration vectors of the particle i with respect to $\mathcal{F}$, respectively. G is the gravitational acceleration vector. T is the moment vector acting on the contact point p. r_j denotes the position vector of the particle j with respect to $\mathcal{F}$. F_j and M_j denote the force and the moment vectors acting on the particle j relative to the frame $\mathcal{F}$, respectively.

Let the ZMP be on the point p. The moment T will be a zero vector by the ZMP concept. Therefore, equation (5) can be rewritten relative to the moving frame $\bar{\mathcal{F}}$ as follows:

$$\sum_{i=1}^{n} m_i(\bar{r}_i - \bar{r}_{zmp}) \times (\ddot{\bar{r}}_i + \ddot{r}_q + G + \dot{\bar{\omega}} \times \bar{r}_i + 2\bar{\omega} \times \dot{\bar{r}}_i + \bar{\omega} \times (\bar{\omega} \times \bar{r}_i))$$
$$- \sum_{j=1}^{n}((\bar{r}_j - \bar{r}_{zmp}) \times \bar{F}_j + \bar{M}_j) = 0, \tag{6}$$

where $\bar{r}_{zmp}$ is the position vector of the ZMP with respect to $\bar{\mathcal{F}}$. r_q is the position vector of the origin of $\bar{\mathcal{F}}$ from the origin of $\mathcal{F}$. $\bar{\omega}$ and $\dot{\bar{\omega}}$ denote the angular velocity and acceleration vectors, respectively.

In case that the upper body is modeled as a four-mass model as shown in Figure 8, three moment components generated by the motion of the particles of the legs, M = $[M_x\ M_y\ M_z]T$, can be written as follows:

$$m_s(\bar{z}_s\ddot{\bar{x}}_s - \bar{x}_s\ddot{\bar{z}}_s) + m_t(\bar{z}_t - \bar{z}_{zmp})(\ddot{\bar{x}}_t + \ddot{x}_q + g_x)$$
$$- m_t(\bar{x}_t - \bar{x}_{zmp})(\ddot{\bar{z}}_t + \ddot{z}_q + g_z)$$
$$+ m_w(\bar{z}_w - \bar{z}_{zmp})(\ddot{\bar{x}}_w + \ddot{x}_q + g_x)$$
$$- m_w(\bar{x}_w - \bar{x}_{zmp})(\ddot{\bar{z}}_w + \ddot{z}_q + g_z) = -M_y(t), \tag{7}$$

$$m_s(\bar{y}_s\ddot{\bar{z}}_s - \bar{z}_s\ddot{\bar{y}}_s) + m_t(\bar{y}_t - \bar{y}_{zmp})(\ddot{\bar{z}}_t + \ddot{z}_q + g_z)$$
$$- m_t(\bar{z}_t - \bar{z}_{zmp})(\ddot{\bar{y}}_t + \ddot{y}_q + g_y)$$
$$+ m_w(\bar{y}_w - \bar{y}_{zmp})(\ddot{\bar{z}}_w + \ddot{z}_q + g_z)$$
$$- m_w(\bar{z}_w - \bar{z}_{zmp})(\ddot{\bar{y}}_w + \ddot{y}_q + g_y) = -M_x(t), \tag{8}$$

$$m_s(\bar{x}_s\ddot{\bar{y}}_s - \bar{y}_s\ddot{\bar{x}}_s + 2(\bar{x}_s\dot{\bar{x}}_s + \bar{y}_s\dot{\bar{y}}_s)\bar{\omega}_z + (\dot{\bar{x}}_s^2 + \dot{\bar{y}}_s^2)\dot{\bar{\omega}}_z)$$
$$+ m_t(\bar{x}_t - \bar{x}_{zmp})(\ddot{\bar{y}}_t + \ddot{y}_q + g_y)$$
$$- m_t(\bar{y}_t - \bar{y}_{zmp})(\ddot{\bar{x}}_t + \ddot{x}_q + g_x)$$
$$+ m_w(\bar{x}_w - \bar{x}_{zmp})(\ddot{\bar{y}}_w + \ddot{y}_q + g_y)$$
$$- m_w(\bar{y}_w - \bar{y}_{zmp})(\ddot{\bar{x}}_w + \ddot{x}_q + g_x) = -M_z(t), \tag{9}$$

where m_s denotes the mass of both shoulders including the mass of the arms. m_t is the mass of the torso including the head, shoulders and arms, and m_w is the mass of the waist. $\bar{r}_t = [\bar{x}_t\ \bar{u}_t\ \bar{z}_t]^T$ and $\bar{r}_w = [\bar{x}_w\ \bar{u}_w\ \bar{z}_w]^T$ are the position vectors of the neck and the waist with respect to the $\bar{\mathcal{F}}$, respectively. $\bar{r}_s = [\bar{x}_s\ \bar{y}_s\ \bar{z}_s]^T$ is the position vector of the shoulder with respect to the neck frame.
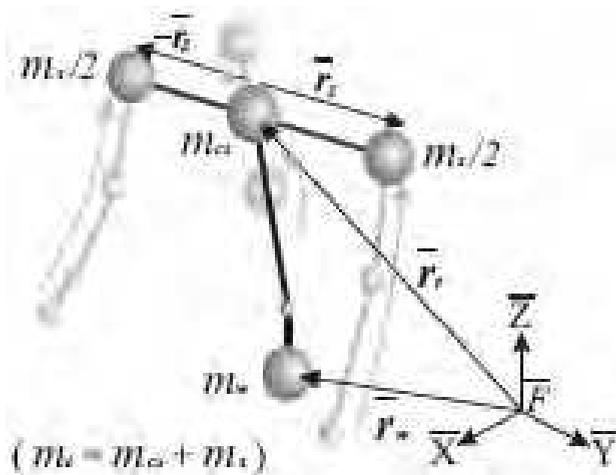
Fig. 8. Approximate model of upper body.

These moment equations are interferential and non-linear because each equation has the same variables, $\bar{z}_w$ and $\bar{z}_t$. Thus, it is difficult to derive analytic solutions from equations (7), (8) and (9). We assume that neither the waist nor the trunk particles move vertically, and the trunk arm rotates on the horizontal plane only as

$$\ddot{\bar{z}}_t = 0, \; \ddot{\bar{z}}_w = 0, \; \ddot{\bar{z}}_q = 0, \; \bar{z}_t - \bar{z}_{zmp} = const., \; \bar{z}_w - \bar{z}_{zmp} = const. \tag{10}$$

We put the terms about the motion of the particles of the upper body on the left-hand side as unknown variables, and the terms about the moments generated by the particles of the lower-limbs on the right-hand side as known parameters. The decoupled and linearized ZMP equations can be written as

$$\hat{M}_{yt} + \hat{M}_{yw} = \hat{M}_y(t), \tag{11}$$

$$\hat{M}_{xt} + \hat{M}_{xw} = \hat{M}_x(t), \tag{12}$$

$$m_t l^2 \theta_t = \hat{M}_z(t), \tag{13}$$

where

$$\hat{M}_{yt} = m_t(\bar{z}_t - \bar{z}_{zmp})\ddot{\bar{x}}_t - m_t g_z \bar{x}_t,$$
$$\hat{M}_{yw} = m_w(\bar{z}_w - \bar{z}_{zmp})\ddot{\bar{x}}_w - m_w g_z \bar{x}_w,$$
$$\hat{M}_{xt} = -m_t(\bar{z}_t - \bar{z}_{zmp})\ddot{\bar{y}}_t + m_t g_z \bar{y}_t,$$
$$\hat{M}_{xw} = -m_w(\bar{z}_w - \bar{z}_{zmp})\ddot{\bar{y}}_w + m_w g_z \bar{y}_w,$$
$$\hat{M}_y(t) = -M_y - (m_t(\bar{z}_t - \bar{z}_{zmp})\ddot{x}_q + m_t g_z \bar{x}_{zmp}$$
$$+ m_w(\bar{z}_w - \bar{z}_{zmp})\ddot{x}_q + m_w g_z \bar{x}_{zmp}),$$
$$\hat{M}_x(t) = -M_x - (-m_t(\bar{z}_t - \bar{z}_{zmp})\ddot{y}_q - m_t g_z \bar{y}_{zmp} \tag{14}$$

$$-m_w(\bar{z}_w - \bar{z}_{zmp})\ddot{y}_q - m_w g_z \bar{y}_{zmp}),$$
$$\hat{M}_z(t) = -M_z - (m_t(\bar{x}_t - \bar{x}_{zmp})(\ddot{\bar{y}}_t + \ddot{y}_q)$$
$$-m_t(\bar{y}_t - \bar{y}_{zmp})(\ddot{\bar{x}}_t + \ddot{x}_q)$$
$$+m_w(\bar{x}_w - \bar{z}_{zmp})(\ddot{\bar{y}}_w + \ddot{y}_q)$$
$$-m_w(\bar{y}_w - \bar{y}_{zmp})(\ddot{\bar{x}}_w + \ddot{x}_q),$$

where θ_t is the vertical angle of the trunk. l is the length between the neck and the shoulder. $\hat{M}_{xt}$ and $\hat{M}_{yt}$ denote the roll's and the pitch's trunk components of the moments, respectively. $\hat{M}_{xw}$ and $\hat{M}_{yw}$ the moment components of the waist's roll and pitch, respectively.

$\hat{M}_{xw}$, $\hat{M}_{yw}$, $\hat{M}_{xt}$ and $\hat{M}_{yt}$ become the known functions because they are calculated by the motion of the lower-limbs and the time trajectory of the ZMP. In steady walking, they are periodic functions because each particle of the biped humanoid robot and the ZMP move periodically with respect to the frame $\bar{\mathcal{F}}$. Comparing the Fourier transform coefficients of both sides of each equation, the approximate periodic solutions of the pitch's and roll's waist and trunk, $\bar{y}_w$, $\bar{x}_w$, $\bar{y}_t$, $\bar{x}_t$ and θ_t can be obtained.

4.3 Recursive Calculation

It is difficult to calculate the compensatory motion due to six unknown variables such as $\bar{y}_w$, $\bar{x}_t$, $\bar{y}_t$, θ_t and θ_w. Each equation is represented as a Fourier series. Using the Fourier transform coefficients, the approximate periodic solutions of the pitch's and roll's waist and trunk can be obtained. The approximate solutions are substituted into the moment equation (6), and the errors of moments generated by the waist and trunk motions are calculated according to the planned ZMP. These errors are accumulated to the right-hand side of equations (11), (12) and (13). The approximate solutions are computed again. These computations are repeated until the errors fall below a certain tolerance level. As a result, the strict periodic solutions of the nonlinear equations are obtained by a convergent regularity. The limit value of an accumulated moment error on each axis, E_n, is estimated as follows:

$$E_n = \frac{2E_{n-1} + e_{n-1}}{2}$$
$$n = 3, 4, 5, ..., \quad E_1 = 0, \quad E_2 = e_1. \tag{15}$$

where e_n is the nth moment error.

Figure 9 shows the block diagram for the compensatory motion of the waist and trunk. We numerically verified the convergence of the solutions using computer simulations. A 30 deg turning walking was simulated with the step time of 1.28 s/step and the step width of 0.2 m/step. Among the ten, the biped humanoid robot turned at the fifth and sixth step. Figure 10 shows the convergence of the turning walking. In this simulation, the errors of the pitch's, roll's and yaw's moments drop below 0.1 Nm after ten iterations.

Figure 11 shows the convergence of the trunk motion depending on the walking speed when the trunk length is 0.6[m]. In these simulations, the errors of the ZMP are dropped below 1.0[mm]. We can see that the recursive method does not take so much time in calculating the compensatory motion of the trunk and waist.
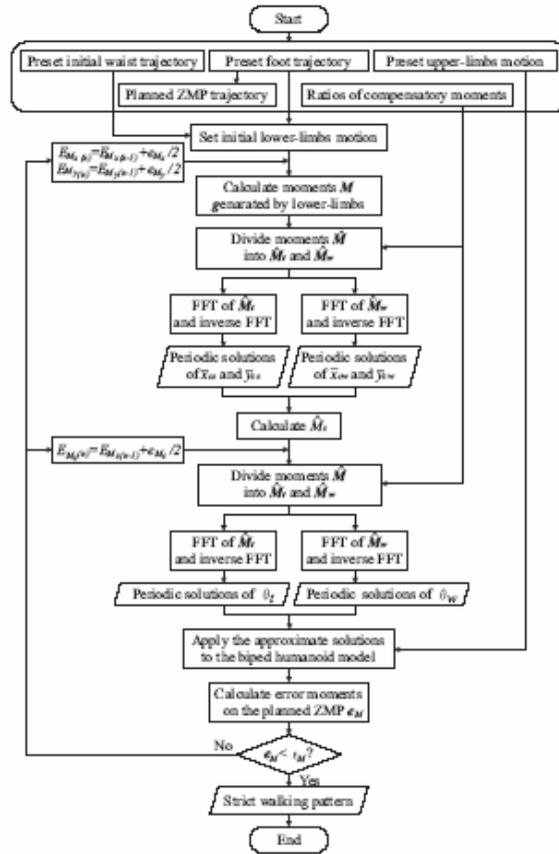
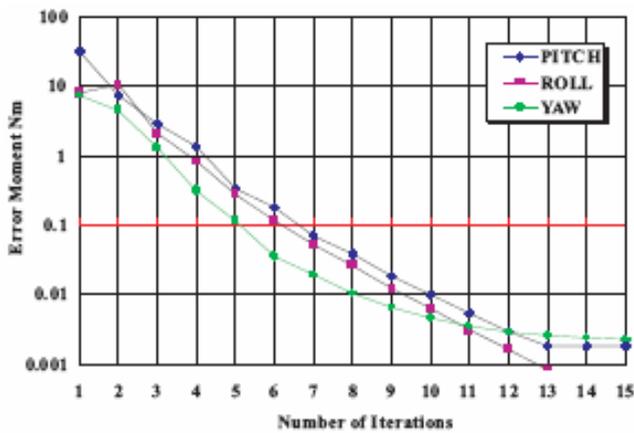Fig. 9. Calculation of compensatory motion.
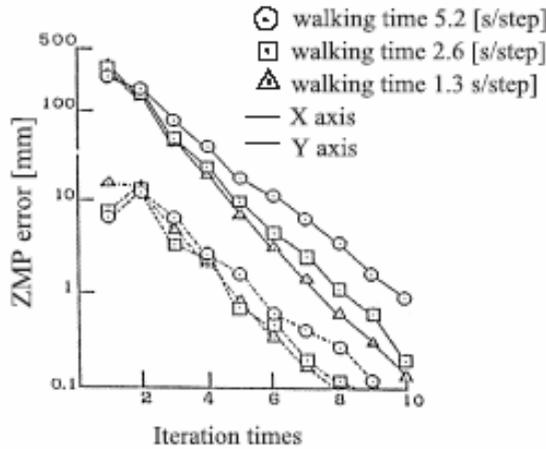

Fig. 10. Moment errors in turning walking.

Fig. 11. Convergence of trunk

4.4 Trunk Motion for Complete Walking

This compensation control is also applicable to a complete walking. By regarding the complete walking motion as one periodic walking motion and applying the control method to it, the compensatory motion of the waist and trunk in steady and transitional walking can be derived. However, the biped humanoid robot must have a long period of standing time before starting and after stopping.

Assuming that the waist is immovable, the pitch's and the roll's moment components of equation (6) can be changed as

$$(\bar{z}_t - \bar{z}_{zmp})\ddot{\bar{x}}_t - g_z\bar{x}_t = -A(t), \tag{16}$$

$$(\bar{z}_t - \bar{z}_{zmp})\ddot{\bar{y}}_t + g_z\bar{y}_t = B(t), \tag{17}$$

where

$$A(t) = \frac{M_y(t) + m_w(\bar{z}_w - \bar{z}_{zmp})\ddot{\bar{x}}_w - m_w g_z\bar{x}_w}{m_t},$$

$$B(t) = \frac{M_x(t) - m_w(\bar{z}_w - \bar{z}_{zmp})\ddot{\bar{y}}_w - m_w g_z\bar{y}_w}{m_t} \tag{18}$$

Consider only the motion of the trunk around the pitch's axis to investigate the compensatory motion. The transfer function $\bar{y}_t(\omega)$ in the frequency domain can be expressed as

$$\bar{y}_t(\omega) = \frac{2p}{\omega^2 + p^2}q = \left(\frac{1}{p - j\omega} + \frac{1}{p + j\omega}\right)q, \tag{19}$$

where

$$p = \sqrt{\frac{g_z}{\bar{z}_t - \bar{z}_{zmp}}}, \quad q = -\frac{1}{2g_z}\sqrt{\frac{g_z}{\bar{z}_t - \bar{z}_{zmp}}}. \tag{20}$$

According to the ZMP concept, $\bar{z}_{zmp}$ in equation (20) is zero. Equation (19) is generally known as Lorentz function, and its primitive function is written as

$$\bar{y}_t(t) = qe^{-p|t|}.$$

(21)

We can imagine from equation (21) that the casual law may not be applied anymore. If the walking speed of the biped humanoid robot is increased, it goes without saying that $\bar{y}_t(t)$ affects stability more badly. The trunk, therefore, should be in motion earlier than the shift of the ZMP on the ground to cancel the moments produced.

The relationship between the motion of the trunk and the applied force was simulated. When the biped humanoid robot was not in motion, an impulse moment 1000 Nm was applied to the trunk's pitch. Figure 12 shows the pitch's motion of the trunk. In this simulation, we can see that the compensatory motion of the trunk should begin with a view of balancing before and after the impulse moment is applied to the biped humanoid robot.
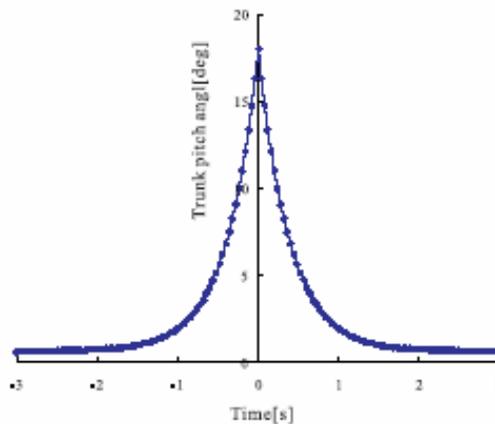

Fig. 12. Motion of trunk's pitch

5. Impedance Control

It is difficult for a biped humanoid robot to avoid instability caused by the impact/contact forces produced between the landing foot and the ground during dynamic walking. So, an impedance control is discussed in this section to guarantee higher stability with high speed walking (Lim *et al.*, 2004c)

When a human walks, he controls his leg muscles for shock absorption and posture. His muscles are relaxed to absorb the impact/contact force just before his landing foot makes an initial contact, while his muscles are hardened to maintain the balance after landing (Kazerooni & Waibel, 1988; Park & Kim, 1999). We pay attention to the elasticity of the biped humanoid robot like a human.

Suppose that the biped foot is connected to the ground with a spring and a damper model. A force/torque sensor is mounted between the foot and the ankle to measure the impact/contact force as shown in Figure 13. Also, an ankle coordinate frame F_a is fixed on the center of the ankle, and an end-effector coordinate frame F_z is attached at the ZMP.

The impact/contact force between the landing foot and the ground, $F \in \Re^6$, can be written as

$$M_d \ddot{p} + D_d \dot{p}_e + K_d p_e = F,$$
$$p_e = p - p_d,$$

(22)

where $M_d \in \Re^{6 \times 6}$ is the desired mass matrix. $D_d \in \Re^{6 \times 6}$ and $K_d \in \Re^{6 \times 6}$ are the damping and stiffness matrices, respectively. $p \in \Re^6$ and $p_d \in \Re^6$ denote the actual and desired position vectors of the foot, respectively. The joint angles of the leg can be measured by the proper encoders attached to each joint. Then, p is calculated by forward kinematics. The reaction force F is measured by the force/torque sensor.
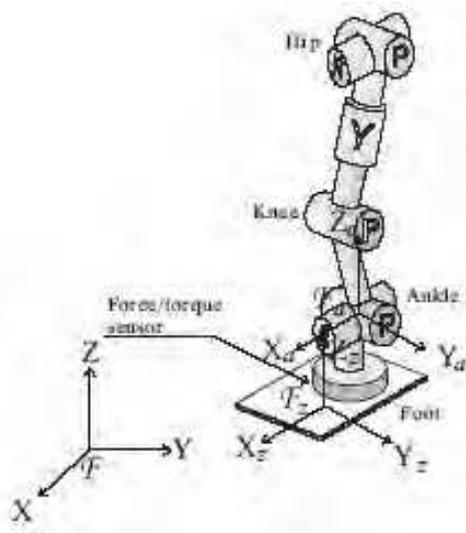
Fig. 13. Ankle and ZMP coordinate frames.

The angular velocity vector $\dot{\theta}_e$ that is commanded to the landing leg can be obtained as follows:

$$\dot{\theta}_e = J^{-1}(\theta) \dot{p}$$

(23)

where

$$\dot{p} = M_d^{-1} \int (F - D_d \dot{p}_e - K_d p_e).$$

(24)

For the absorption of the impact forces and the stable posture of the biped humanoid robot, an impedance control method is employed as shown in Figure 14. During the whole walking cycle, the position control based on the walking pattern is basically employed. The joint angles are measured by the encoders, and the actual position of the foot is calculated by using forward kinematics. The parameters in the impedance control are modulated depending on the gait phase as follows:
(1) in the swinging phase, only the position control is employed,(2) in the contact/double supporting phase, the impedance control with large viscosity is employed to reduce the impact/contact force, (3) in the first half of the single sup-porting phase, the impedance

control with large stiffness is applied to increase the momentum reduced, and (4) in the last half of the single supporting phase, the walking pattern changed by the impedance control is interpolated to the desired walking pattern.
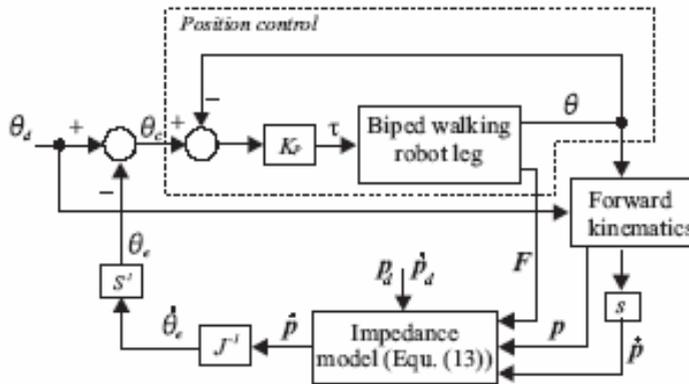

Fig. 14. Impedance control systems.

6. Experiments

For a biped humanoid robot to walk stably on terrains, the moment compensation control and the impedance control were described in the above sections. In this section, the effectiveness of the control methods is tested through dynamic walking experiments.

6.1 Impedance Control Test

The position control and the impedance control are experimented using a WABIAN serious robot. In this experiment, the impedance control was applied to the ankle joint. Dynamic walking is realized with the step speed of 1.28 s/step and the step length of 0.15 m/step (Lim *et al.*, 2004c).
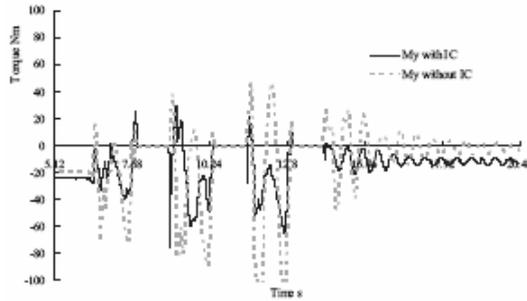
The contact forces and moments of the left foot are shown in Figure 15 (a)-(b), respectively. The experimental results are plotted after 5.12 s. The pitch's contact forces and moments are largely reduced in the last step. Figure 16 (a) and (b) illustrate the desired and actual x-and y-ZMP. The ZMP errors in the impedance control are small. So, we can say that the position-based impedance control is effective in suppressing the impact/contact forces and moments.

6.2 Compensation Control Test

The walking direction and length can be determined by a vision tracking and an auditory system (Lim *et al.*, 2004b). The vision system is initialized, and both hands of a human are specified as tracking points during the walking. The auditory system recognizes the walking length that is defined by compiling the text file of grammar rules. Using the locomotion pattern generator based on the visual and the auditory information, a locomotion pattern with 25 steps (four steps forwards, five steps to the right, four steps backwards, six steps to the left and six steps on the spot) is created.
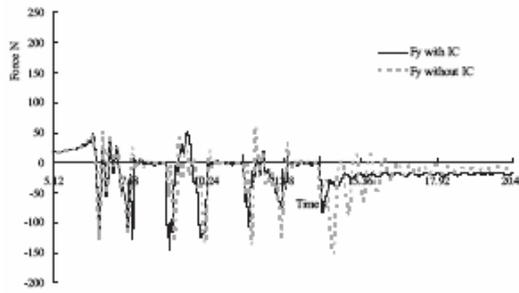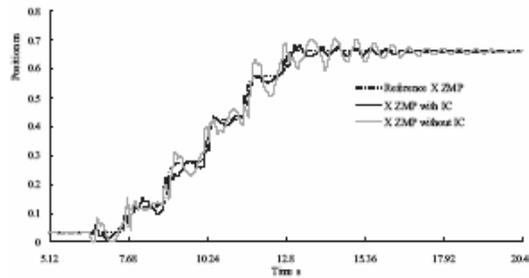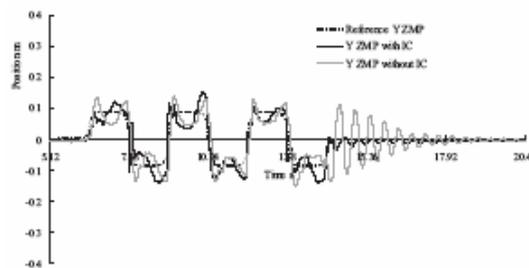
(b) Pitch's reaction force F_y.

(a) Pitch's moment M_y.

Fig. 15. Reaction forces and Moments on the left foot. IC denotes the impedance control.


(a) X-ZMP

(b) Y-ZMP

Fig. 16. ZMP trajectories under two different controls. IC: Impedance control.

In the experiment, dynamic walking with 25 steps was achieved with the walking speed of 0.96 s/step using the moment compensation control. The response trajectories show a good accuracy of following the reference joint trajectories as shown in Figure 17. It means that the compensatory motion of the waist and trunk is used effectively.
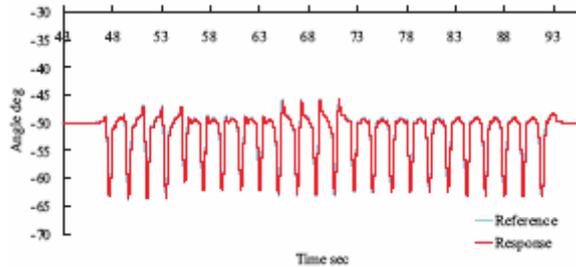
(a) Pitch's angle of knee joint.
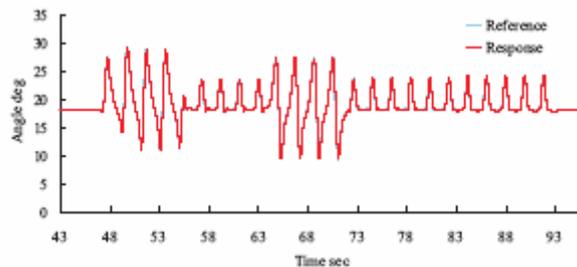
(b) Pitch's angle of hip joint.

Fig. 17. Angle response of the right leg.

7. Conclusion and Discussion

The mechanism of a 43 DOF biped humanoid robot WABIAN-RII was described to simulate human motions was described. For the humanoid robot to walk stably on various terrains, its functions should be separated. Its waist and trunk carries out the function of stability, while its legs work out the function of the locomotion. A locomotion pattern generation was discussed which used a polynomial. In the pattern generation, the direction of the walking and the length of the step can be determined by visual and auditory information. Also, a moment compensation control was presented to balance its body, which was based on the motion of the waist and trunk. In addition, an impedance control method was discussed to absorb the impact/contact forces generated between the landing foot and the ground, which can adjust the impedance parameters to make relaxed and hardened motions like a human.

The experimental results show that the impedance and the moment compensation control are effective for the sock absorption and stability. However, for a more reliable locomotion, biped humanoid robots must be able to adjust the time of the locomotion. If the walking time is suddenly changed, unnecessary acceleration is able to occur, and the errors of the ZMP can be increased. To solve these problems, a new control method will be introduced which uses the motion of the upper-limbs, and the impedance control should be considered in all the joints. Especially, the moment of the yaw should be compensated to deal with high speed walking.

7. References

Kato, I.; Ohteru, S.; Kobayashi, H.; Shirai, K. & Uchiyama, A. (1973). Information-power machine with senses and limbs, *Proc. CISM-IFToMM Symp. On Theory and Practice of Robots and Manipulators*, pp. 12-24

Takanishi, A.; Ishida, M.; Yamazaki, Y. & Kato, I. (1985). The realization of dynamic walking by the biped walking robot, *Proc. IEEE Int. Conf. on Robotics and Automation*, pp. 459-466

Takanishi, A.; Egusa, Y.; Tochizawa, M.; Takebayashi, T. & Kato, I. (1988). Realization of dynamic walking stabilized with trunk motion, *Proc. CISM-IFToMM Symp. On Theory and Practice of Robots and Manipulators*, pp. 68-79

Li, Q.; Takanishi, A. & Kato, I. (1992). Learning control of compensative trunk motion for biped walking robot based on ZMP stability criterion, *Proc. IEEE/RSJ Int. Conf. on Intelligent Robots and Systems*, pp. 597-603

Yamaguchi, J.; Takanishi, A. & Kato, I. (1995). Experimental development of a foot mechanism with shock absorbing material for acquisition of landing surface position information and stabilization of dynamic biped walking, *Proc. IEEE Int. Conf. on Robotics and Automation*, pp. 2892-2899

Takanishi, A.; Lim, H.; Tsuda M. & Kato I. (1990). Realization of dynamic biped walking stabilized by trunk motion on a sagittally uneven surface, *Proc. IEEE/RSJ Int. Workshop on Intelligent Robots and Systems*, pp. 323-329

Takanishi, A.; Kumeta, M.; Matsukuma, K.; Yamaguchi, J. & Kato, I. (1991). Development of control method for biped walking under unknown external force acting in lateral plane *RSJ Annual Conf. on Robotics*, pp. 321-3224

Setiawan, S.; Hyon, S.; Yamaguchi, J. & Takanishi, A. (1999). Physical interaction between human and a bipedal humanoid robot: realization of human-follow walking *Proc. IEEE Int. Conf. on Robotics and Automation*, pp. 361-367

Lim, H.; Ishii A. & Takanishi A. (2004a). Emotion-based biped walking, *Int. J. Information, Education and Research in Robotics and Artificial Intelligence*, Vol.22, No.5, pp.577-586
Lim, H.; Kaneshima, Y. & Takanishi, A. (2004*b*). Online walking pattern and balance motion for a biped humanoid robot having a trunk, *Int. J. Human-friendly Welfare Robotic Systems*, Vol.5, No.1, pp. 26-35

Lim, H. & Takanishi A. (2005). Compensatory motion control for a biped walking robot, *Proc. Int. J. Information, Education and Research in Robotics and Artificial Intelligence*, Vol.23, No.1, pp.1-11

Vukobratovic M., Frank A. & Juricic D. (1970). On the stability of biped locomotion, *IEEE Trans. Biomedical Engineering*, vol. 17, no. 1, pp. 25-36

Lim H., Setiawan S. & Takanishi A. (2004c). Position-based Impedance Control of Biped Humanoid Robot, *Int. J. Advanced Robotics*, Vol.18, No.4, pp.415-435

Kazerooni K. & Waibel B. (1988). Theory and experiment on the stability of robot compliance control *Proc. IEEE Int. Conf. on Robotics and Automation*, pp. 71-87

Park J. & Cho H, (2000). An online trajectory modifier for the base link of biped robots to enhance locomotion stability, *Proc. IEEE Int. Conf. on Robotics and Automation*, pp. 3353-3358

Mobile Robotics, Moving Intelligence

Edited by Jonas Buchli

This book covers many aspects of the exciting research in mobile robotics. It deals with different aspects of the control problem, especially also under uncertainty and faults. Mechanical design issues are discussed along with new sensor and actuator concepts. Games like soccer are a good example which comprise many of the aforementioned challenges in a single comprehensive and in the same time entertaining framework. Thus, the book comprises contributions dealing with aspects of the Robotcup competition. The reader will get a feel how the problems cover virtually all engineering disciplines ranging from theoretical research to very application specific work. In addition interesting problems for physics and mathematics arises out of such research. We hope this book will be an inspiring source of knowledge and ideas, stimulating further research in this exciting field. The promises and possible benefits of such efforts are manifold, they range from new transportation systems, intelligent cars to flexible assistants in factories and construction sites, over service robot which assist and support us in daily live, all the way to the possibility for efficient help for impaired and advances in prosthetics.

How to reference

In order to correctly reference this scholarly work, feel free to copy and paste the following:

Hun-ok Lim and Atsuo Takanishi (2006). Mechanism and Control of Anthropomorphic Biped Robots, Mobile Robotics, Moving Intelligence, Jonas Buchli (Ed.), ISBN: 3-86611-284-X, InTech, Available from: http://www.intechopen.com/books/mobile_robotics_moving_intelligence/mechanism_and_control_of_anthropomorphic_biped_robots

INTECH

open science | open minds